Synthesis and characterization of magneto electric coupling in nanostructured $BiFeO_3$and $BiFe1_{-x}MxO3$ (M = Mn, Co, etc.) thin films for spintronics applications

P. Sateesh [a, *], A. Rajesh [a], N. Maramu [b], N. Hemanth [a], K. Gopinath [c], P. Sivakumar [d], T. Satya [e], G. K. Sivasankara Yadav [f], T. Ramprasad [a], M. Rajesh [a]
[a] *Department of Physics, St.Peter'S Engineering College, Secunderabad-500043*
[b] *Department of Physical science, Kakatiya Institute of technology and science, Warangal-506015*
[c] *Department of chemistry, St.Peter'S Engineering College, Secunderabad-500043*
[d] Department of Physics, Kaveri University, Gowraram- 507211, India.
[e] *Department of H&BS, G.Pulla Reddy Engineering College (Autonomous), Kurnool-518007*
[f] *Department of Physics, Rayalaseema university, Kurnool-518007*

In a recent study, researchers employed sol-gel deposition techniques to fabricate both pure BiFeO3 and heterostructured BiFeO3/BiFe1-xMxO3 thin films. The aim was to enhance the magnetic properties of BiFeO3 through doping with Co3+ and Mn3+. The team successfully prepared pure BiFeO3 (BFO) and doped BiFe1-xMxO3 films with varying concentrations of Mn and Co ions. XRD and Raman spectroscopy studies demonstrated that Co3+ and Mn3+ ions successfully substituted Fe3+ ions within the rhombohedral lattice structure of BFO. The pure BiFeO3 films showed stable and consistent responses when exposed to light, achieving an open circuit potential of -0.18 V and a short circuit photocurrent density of -0.024 mA/cm². Additionally, the incorporation of Co3+ and Mn3+ ions led to a decrease in the average particle size. Recent research using Transmission Electron Microscopy (TEM) data has demonstrated that replacing Co3+ and Mn3+ with Fe3+ in Perovskite structures greatly diminishes oxygen defects. This substitution also raises the concentration of Fe3+ ions at the B-site. Complementary X-ray Photoelectron Spectroscopy (XPS) analysis confirms these results, showing improved magnetic properties in the thin film. Notably, the BFMnC0.08 O thin film exhibits a significant increase in both saturation and remanent magnetization at room temperature. Additionally, computational calculations reveal that CO exhibits a strong preference for adsorption on Mn-doped BiFeO3, with an adsorption energy calculated at -1.0494 eV.

(Received May 7, 2025; Accepted August 21, 2025)

Keywords: BiFeO3 thin film, Perovskite grid, Photo illumination, Spintronics

1. Introduction

Multiferroic materials have become a focal point of research due to their unique physical characteristics and their potential use in devices such as sensors, memory storage, and spintronic components. These materials are categorized into two primary groups: type-I and type-II multiferroics. Type-I multiferroics are notable for their strong ferroelectric properties, though the temperatures at which their magnetic and ferroelectric transitions occur can often surpass room temperature. In these materials, the magnetoelectric (ME) coupling tends to be weak, as it involves interactions between magnetization and polarization. Ferroelectricity in these compounds can arise through mechanisms such as charge ordering or the displacement of ions or ion groups, commonly observed in transition metal oxides like hexagonal RMnO3.Type-II multiferroic materials, also known as "spin driven ferroelectrics," exhibit magnetic ordering that directly induces ferroelectricity by disrupting inversion symmetry. This phenomenon is attributed to their non-

* Corresponding author:
https://doi.org/10.15251/DJNB.2025.203.975

collinear spin spiral structure, which generates the necessary symmetry breaking. In these materials, macroscopic electric polarization arises from the non-centrosymmetric long-range magnetic order. A prime example is orthorhombic RMnO3, where the temperatures for ferroelectric and magnetic phase transitions are closely aligned, resulting in strong magneto electric (ME) coupling. These materials demonstrate both spontaneous polarization and ant ferromagnetic ordering, with an ant ferromagnetic Néel temperature around 643K and a high ferroelectric Curie temperature near 1103K. Research has explored enhancing the magnetic properties of BiFeO3 through B-site (Fe-site) cation substitution, thereby improving its multiferroic characteristics.

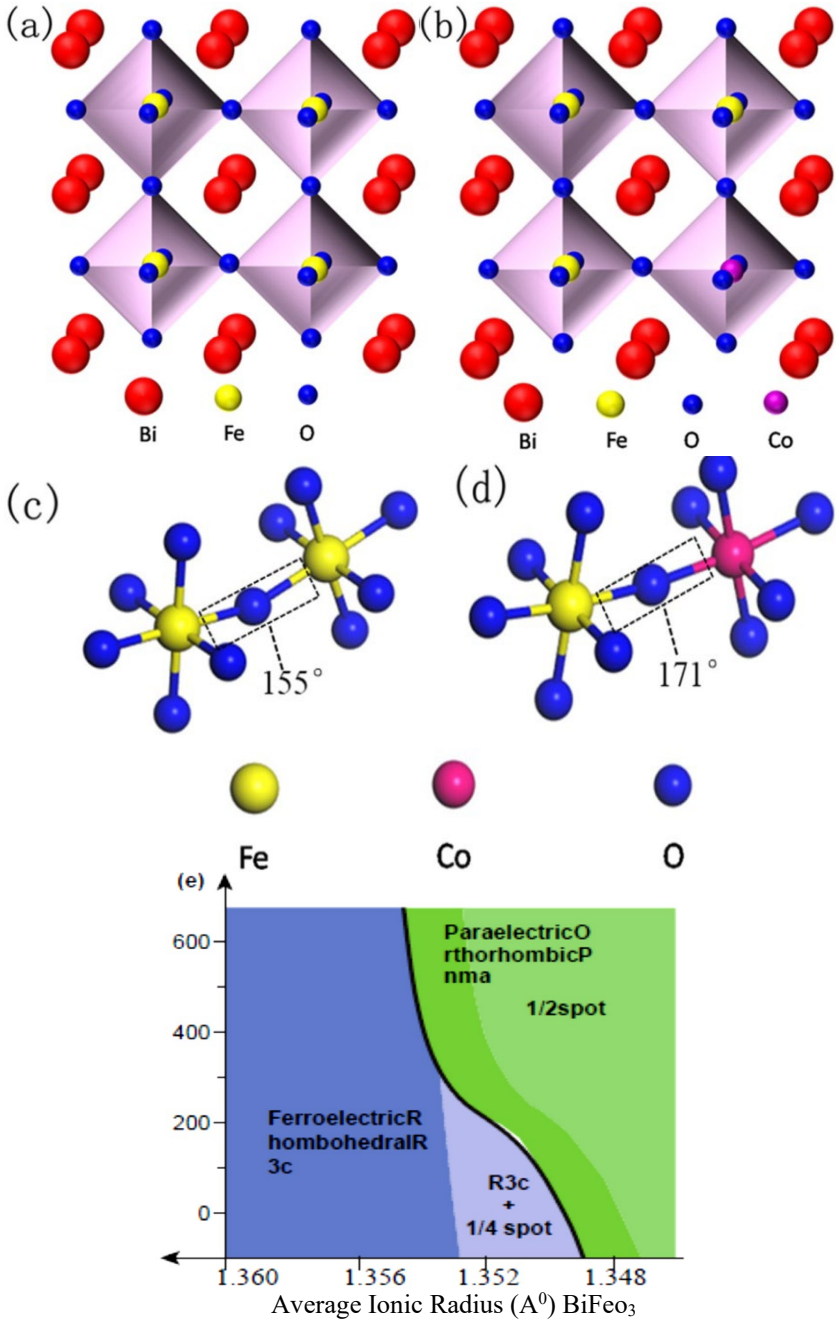

Fig. 1. The simulations included the Polycrystalline BiFeO3 (BFO) crystal structure and the Mn-Co switched BFO. Additionally, the study examined the super-swapping interactions between Fe–O–Fe and Fe–O–Co.

2. Experimental details

Thin films of pure BiFeO3 (BFO) and doped BiFe1-xMxO3 (where M represents elements like Mn or Co, and x values are 0.01, 0.03, 0.06, 0.08, and 0.10) were synthesized on silicon substrates utilizing the sol-gel method. The starting materials, including bismuth nitrate [Bi(NO3)3•5H2O], ferric nitrate [Fe(NO3)3•9H2O], and cobalt (II) nitrate hexahydrate [Co(NO3)2•6H2O], were sourced from Hyderabad, India, and manganese acetate tetrahydrate [Mn(C2H3O2)2•4H2O]. These were fully dissolved in a mixture of glacial acetic acid and ethylene glycol methyl ether to form the precursor solution. Following the precise addition and vigorous agitation of C6H8O7, C2H6O2, and C2H7NO, the solution reached clarity and matured to a 0.4 mol/L concentration over 28 hours. The spin-coating technique involved two phases: an initial spin at 800 rpm for 3 seconds followed by 5000 rpm for 18 seconds. The wet films underwent a pre-annealing process at a temperature of 390°C for a duration of 8 minutes. This procedure was carried out for each layer, allowing for the construction of a film with moderate thickness.The samples underwent a final crystallization step in air at 600°C for one hour before cooling to ambient temperature, resulting in optimal thin films. Figure 2 illustrates the experimental process.

Figure 2 illustrates the procedural diagram for synthesizing BiFe1-xMxO3 thin films, where M represents elements such as Mn or Co. The diagram covers the doping concentrations of x = 0.01, 0.03, 0.06, 0.08, and 0.10, highlighting the integration process for these materials.

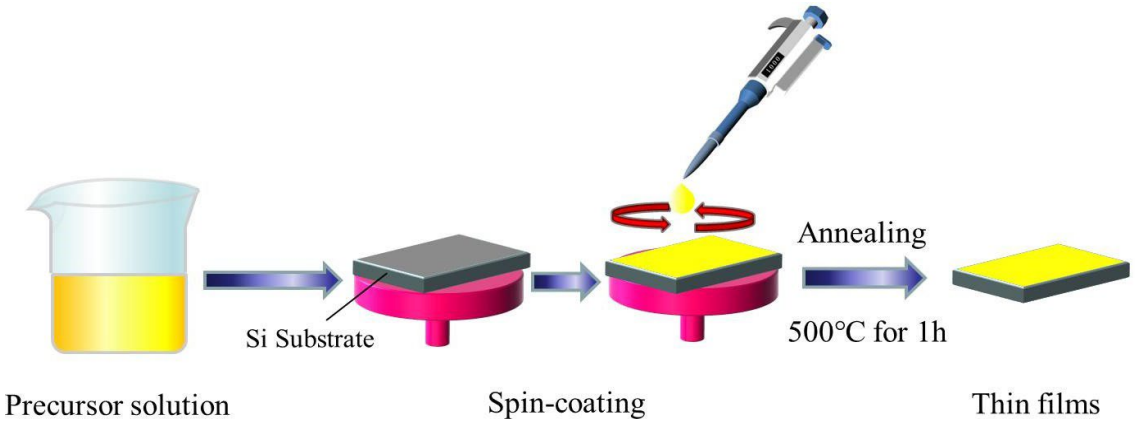

Fig. 2. (e) Phase diagram for rare earth replaced BFO thin films that has been proposed.

3. Results and discussion

To aid in understanding doping principles and super-swapping interactions, figures 3 and 4 simulate the crystal structures of both doped BiFe1-xMxO3 and pure BFO. The BFO composite thin film, which belongs to the space group R3C, displays a deformed rhombohedral Perovskite structure. This structure is characterized by iron ions at the center of an FeO6 octahedron surrounded by six oxygen ions, while bismuth ions form a cube encasing the octahedron. In particular, in Co3+/Mn3+-doped BFO films, one oxygen anion connects two adjacent FeO6/CoO6/MnO3 octahedrons. The difference in size between the B-site cations, specifically Fe3+ and Co3+/Mn3+, causes both dimensional and chemical strain reactions. These reactions disrupt the modulation of the spin cycloid spiral. As a result, some Fe3+ ions are randomly substituted at the B-site. The substitution of Co and Mn ions for Fe ions is clearly demonstrated in Figures 3 and 4 [21]. This substitution leads to the formation of high-energy Co/Mn–O bonds, enhancing the inclination angle of the super-exchange interaction. As a result, the improved super-exchange interaction of Fe–O–Fe (or Mn/Co) contributes to the enhanced magnetic properties of BiFe1-xMxO3, as detailed in the following sections.

The X-ray diffraction (XRD) patterns of the BiFe1-xMxO3 composite thin films, as shown in Figures 3 and 4, exhibit diffraction peaks that align with the standard XRD profile for the rhombohedral phase (space group R3c), as referenced by JCPDS71-2494 and 53-0767. An impurity peak at 28.8◦, attributed to Bi2Fe4O9, is also observed [17,21]. Notably, the disappearance of the (021) peak and shifts in the (012) and (110) peaks around 2θ = 56◦–57.1◦ indicate a structural transition in the BFMO films, from rhombohedral to tetragonal, influenced by Mn doping, consistent with findings from tetragonal BiMnO3 (PDF#53-0767) and corroborated by earlier studies [18].

According to XRD analysis, the intrinsic structures and properties of BiFe1-xMxO3 are unlikely to be significantly affected by the presence of Bi2Fe4O9, owing to its paramagnetic nature and low concentration in the samples [17,21]. The magnified XRD patterns of Co and Mn-substituted thin films at different concentrations are shown in Figure 3b, focusing on the 2θ range of 32◦. An increase in Co3+/Mn3+ concentration results in the diffraction peaks for (104) and (110) moving to higher angles. This shift indicates the effective integration of Co ions into the BFO host lattice. This shift is attributed to the smaller ionic radius of Co3+/Mn3+ compared to Fe3+, resulting in structural deformation and lattice contraction.

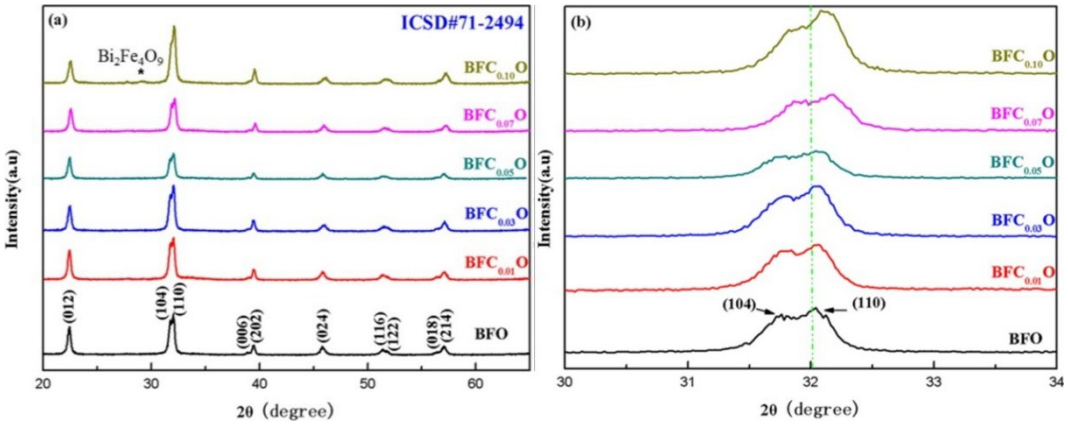

Fig. 3. XRD Patterns of BiFe$_{1-x}$MxO3 (M = Co) and Pure BFO thin films.

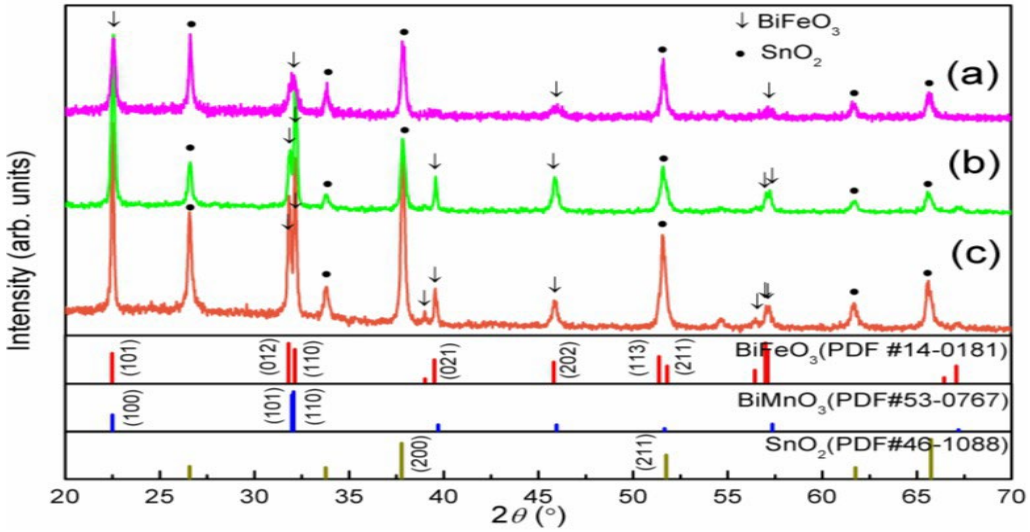

Fig. 4. XRD Patterns of BiFe1-$_x$MxO3 (M = Mn) thin films.

Figure 5a presents the surface and cross-sectional SEM pictures of the BiFe1-xMxO3(M=Mn, Co, etc.) thin films are shown. The Co-substituted thin films are demonstrated to have a consistent surface shape, observable aggregation, and good adhesion to the silicon substrates without apparent separation. Additionally, BiFe1-xMxO3 thin film thicknesses are 308, 293, 288, 261, 223 and 221 nm, respectively, where M is Mn, Co, etc. It appears that Co/Mn doping results in a uniformly dense and grainy surface because the thickness obviously reduces as the amount of Co doping increases [26, 27].

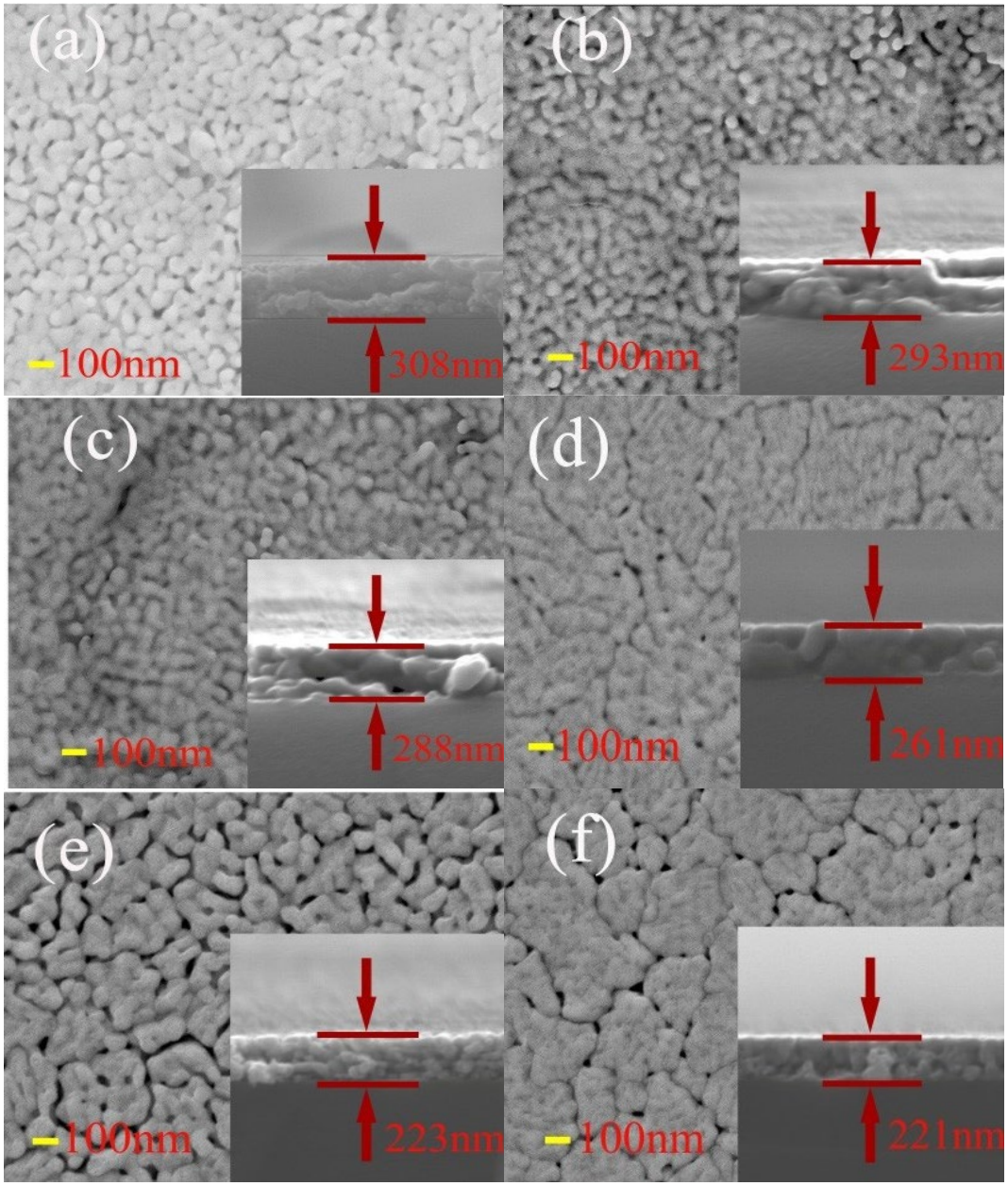

Fig. 5. SEM images illustrating the surface and cross-sectional morphologies of various thin films. These include (a) BFO, (b) BFC/Mn0.010, (c) BFC/Mn0.03O, (d) BFC/Mn0.06O, (e) BFC/Mn0.08O, and (f) BFC/Mn0.10O. These images provide valuable insights into the structural characteristics of each film composition.

4. Magnetic properties

In a magnetic field ranging from 0 to 15 k, we examined how Co and Mn doping affects the magnetic properties of BFO and BiFe 1-xMxO3 thin films (M = Mn, Co, etc.). Figure 8a illustrates the saturated magnetic hysteresis loops observed in both BFO and Co-Mn doped thin films'-Mn tampering with concentration increased saturation magnetization (Ms) as well as remanent magnetization (Mr). The materials BFO, BFC/Mn 0.01 O, BFC/Mn 0.03 O, BFC/Mn 0.05 O, BFC/Mn 0.07 O, and BFC/Mn 0.10 O exhibit the following magnetization values: 21.38 emu/cm³ and 2.06 emu/cm³, 25.57 emu/cm³ and 2.40 emu/cm³, 34.17 emu/cm³ and 2.60 emu/cm³, 34.48 emu/cm³ and 3.00 emu/cm³, 42.38 emu/cm³ and 3.68 emu/cm³, and 47.84 emu/cm³ and 3.43 emu/cm³, respectively. Figure 9 demonstrates the variations in Co doping concentrations between Ms. and Mr. In the case of Ms, the values increase in a linear fashion, whereas Mr initially increases but then decreases as the levels of Co3+ and Mn+3 surpass x = 0.12. The highest recorded value of Mr is 4.64 emu/cm³ at a cobalt concentration of 0.08. In contrast, the maximum value of Ms is 47.88 emu/cm³, which occurs when the doping concentration reaches 0.10.

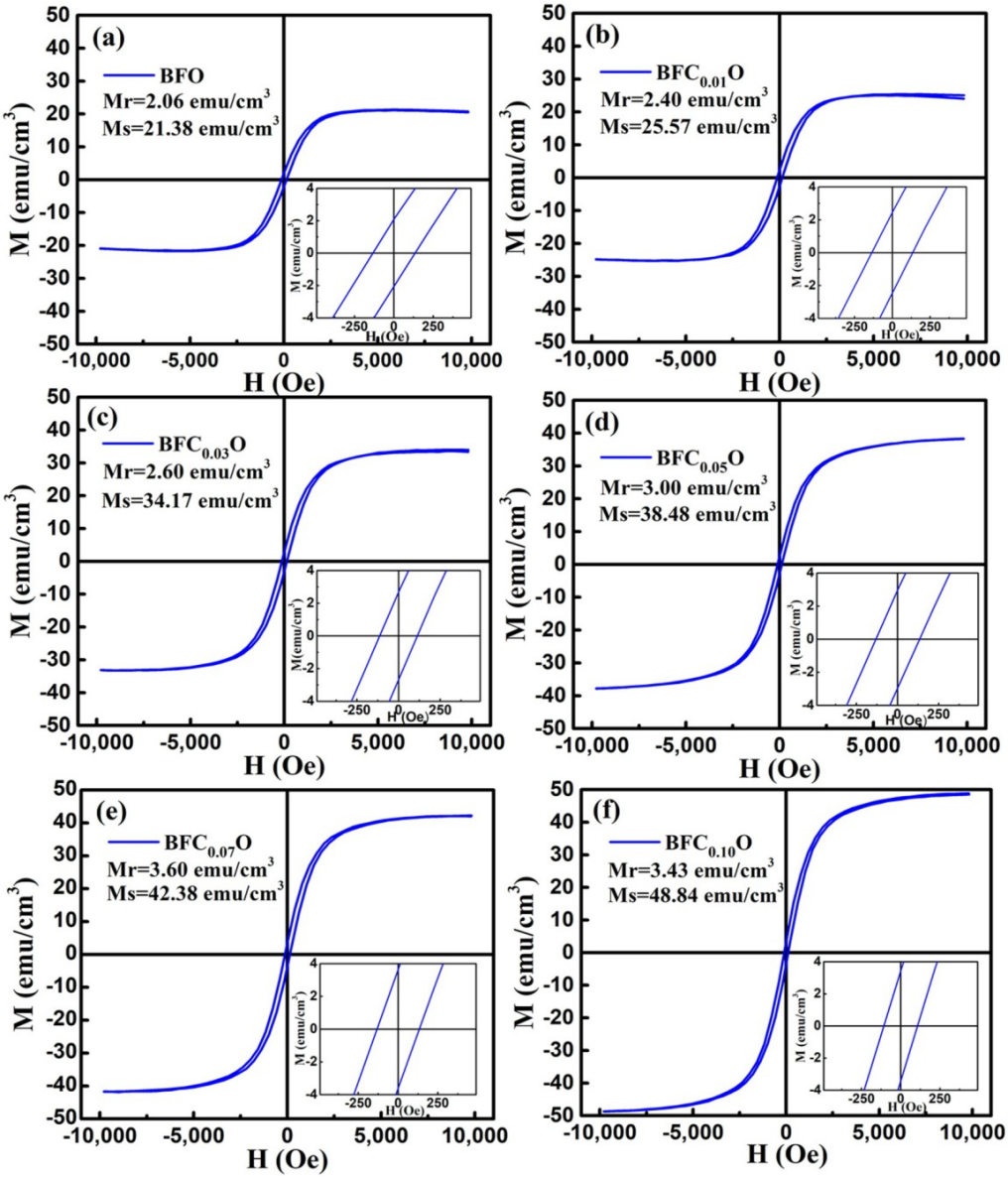

Fig. 8.Presents the magnetic hysteresis (M–H) loops for various room temperature thin films. These include (a) BFO, (b) BFC/Mn0.01O, (c) BFC/Mn0.03O, (d) BFC/Mn0.05O, (e) BFC/Mn0.08O, and (f) BFC/Mn0.10O. Each loop provides insight into the magnetic properties of the films as influenced by differing manganese oxide (MnO) concentrations.

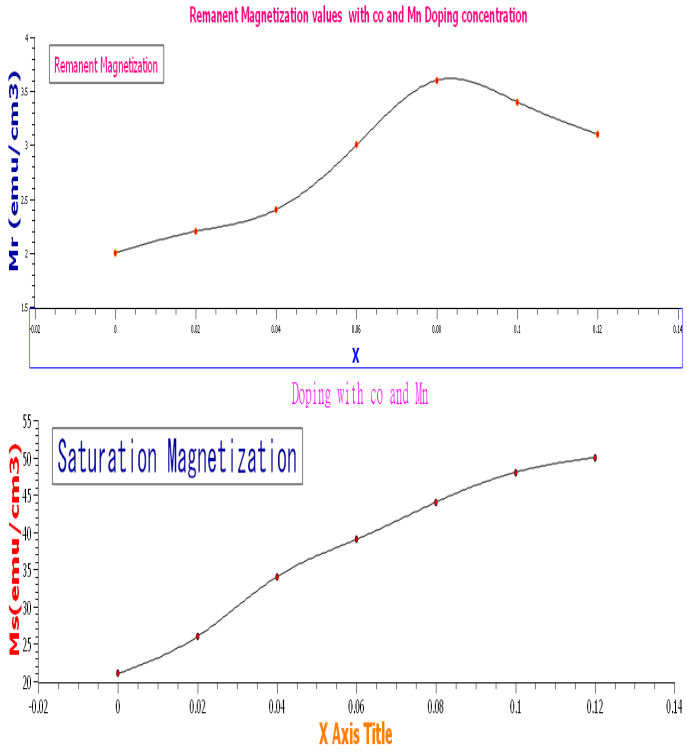

Fig. 9. Variations in saturation magnetization (Ms) and remanent magnetization (Mr) values with concentrations of Co and Mn stupefy.

4.1. Optical properties

The optical characteristics of BFO nanoparticles Current density for BiFe 1 -xMxO3 and BFO thin films (M = Mn, Co, etc., x = 0.01, 0.03, 0.06, 0.08, and 0.10) (b) The photocurrent in BiFe 1-xMxO3 thin-film heating and cooling states at varying light intensities. (c) The output current with BFO and BiFe 1 -xMxO3 (M = Mn, Co) thin films as a function of temperature.

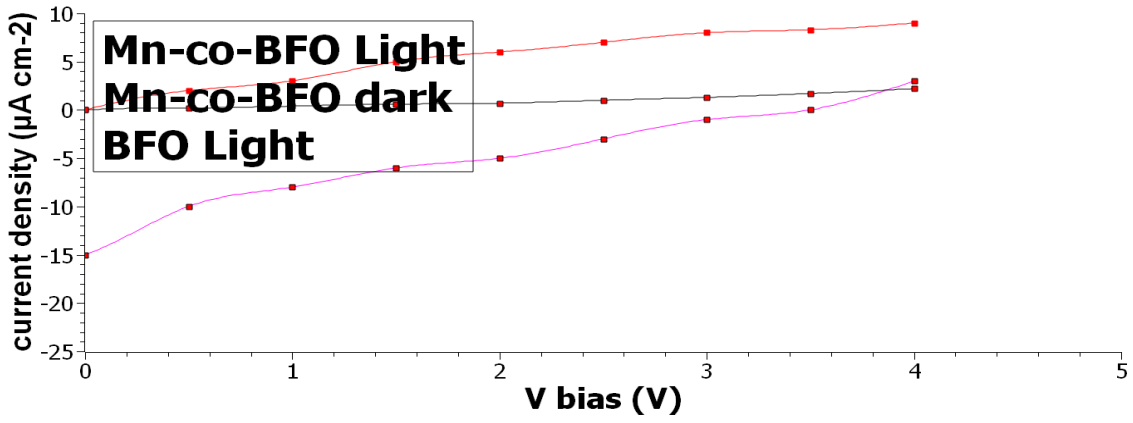

(a)

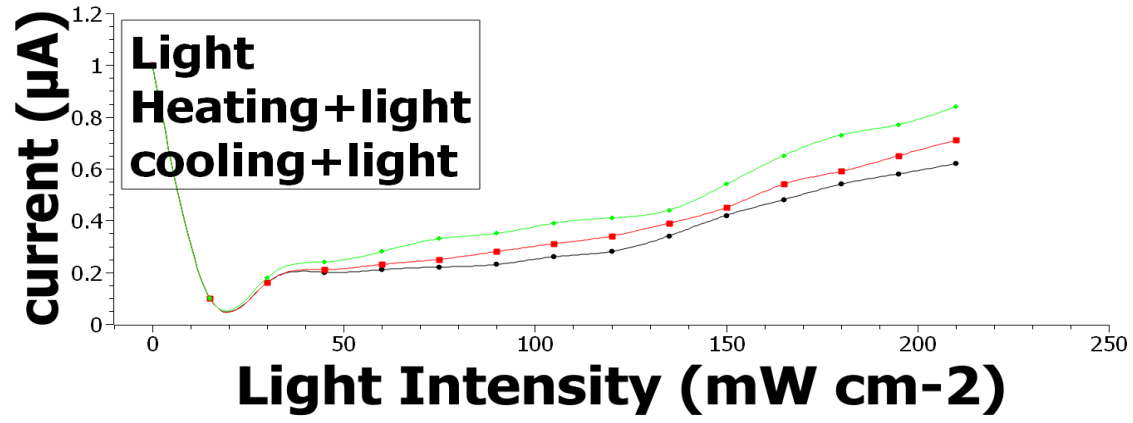

(b)

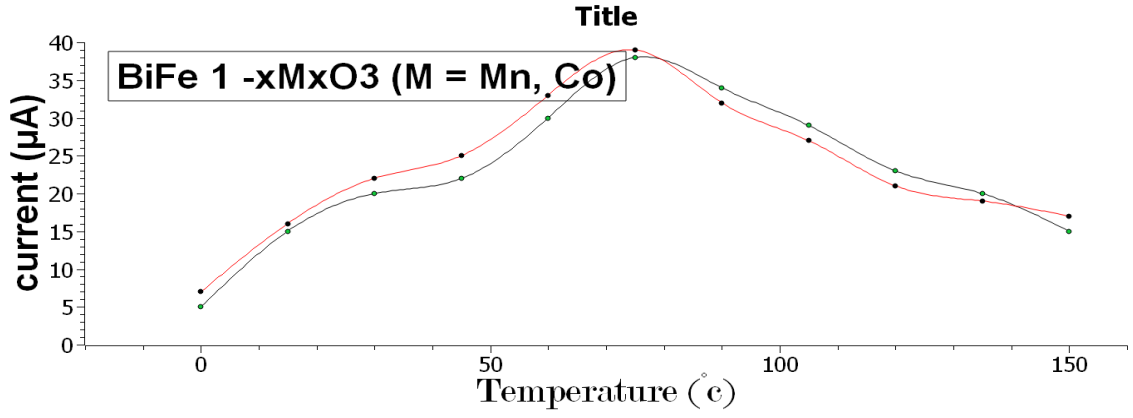

(c)

Fig. 10. (a) Photovoltaic performance for different current densities (b) Photovoltaic current performance for different light intensities (c) Photovoltaic current performance for different temperatures

4.2. Photo catalysis

With a greater light, photocurrent was seen in the heating condition. It was discovered that the cooling state increased the photocurrent under weak light illumination. The photovoltaic properties of BiFe 1-xMxO3 (M = Mn, Co, etc., x = 0.01, 0.03, 0.06, 0.08, and 0.10) thin film materials can be improved using a unique approach, as this work showed that temperature gradients can be used to adjust photovoltaic performance. It is possible for the photocurrent to increase and then drop as the temperature rises. The photo-sensing device's modulated energy bandgap and barrier height are the cause of its temperature-dependent performance.

The aforementioned studies offer fresh perspectives on the photovoltaic effect and offer recommendations for creating high-performance BiFe 1 -xMxO3 (M = Mn, Co) power devices.

4.3. Applications of $BiFe_{1-x}MxO3$ (M = Mn, Co, etc.):

Recent advancements in BFO nanomaterials, specifically those doped with manganese (Mn) and cobalt (Co), have demonstrated promising capabilities in the realm of high-density ferroelectric devices. These materials, which exhibit both ferroelectricity and ferromagnetism at room temperature, offer a unique opportunity to leverage magnetoelectric coupling for advanced applications. Researchers have further explored this potential by developing a magneto resistive device through spin valve exchange, paving the way for innovative applications in electrically written spintronic devices. The study explored a device with a structure that demonstrated a 2% giant magnetoresistance signal, utilizing layers of STO/SRO/BFO-Mn-co/BFO/Mn-CoFeB Cu/Mn-Co. Researchers found that applied voltages could effectively control the exchange bias. However, the weak thermal stability of the BFO/Mn-CoFeB interfaces was a significant barrier to enhancing the magnetoresistance signal. The analysis revealed that the main factor affecting thermal stability was the variation in oxygen vacancies, influenced by the BFO polarization direction. To achieve a higher magnetoresistance value of 4.4%, a new, efficient method was proposed.

4.4. Application for spintronic and optic devices

A) An enormous BFO-based magneto-resistive device. Source: b) swapping coupling with one the ferromagnetic over layer and ant ferromagnetic order for BFO/Mn-co-based spintronic devices, with permission. C) Unidirectional anisotropy using voltage control for Mn-CoFe/BFO heterostructures.

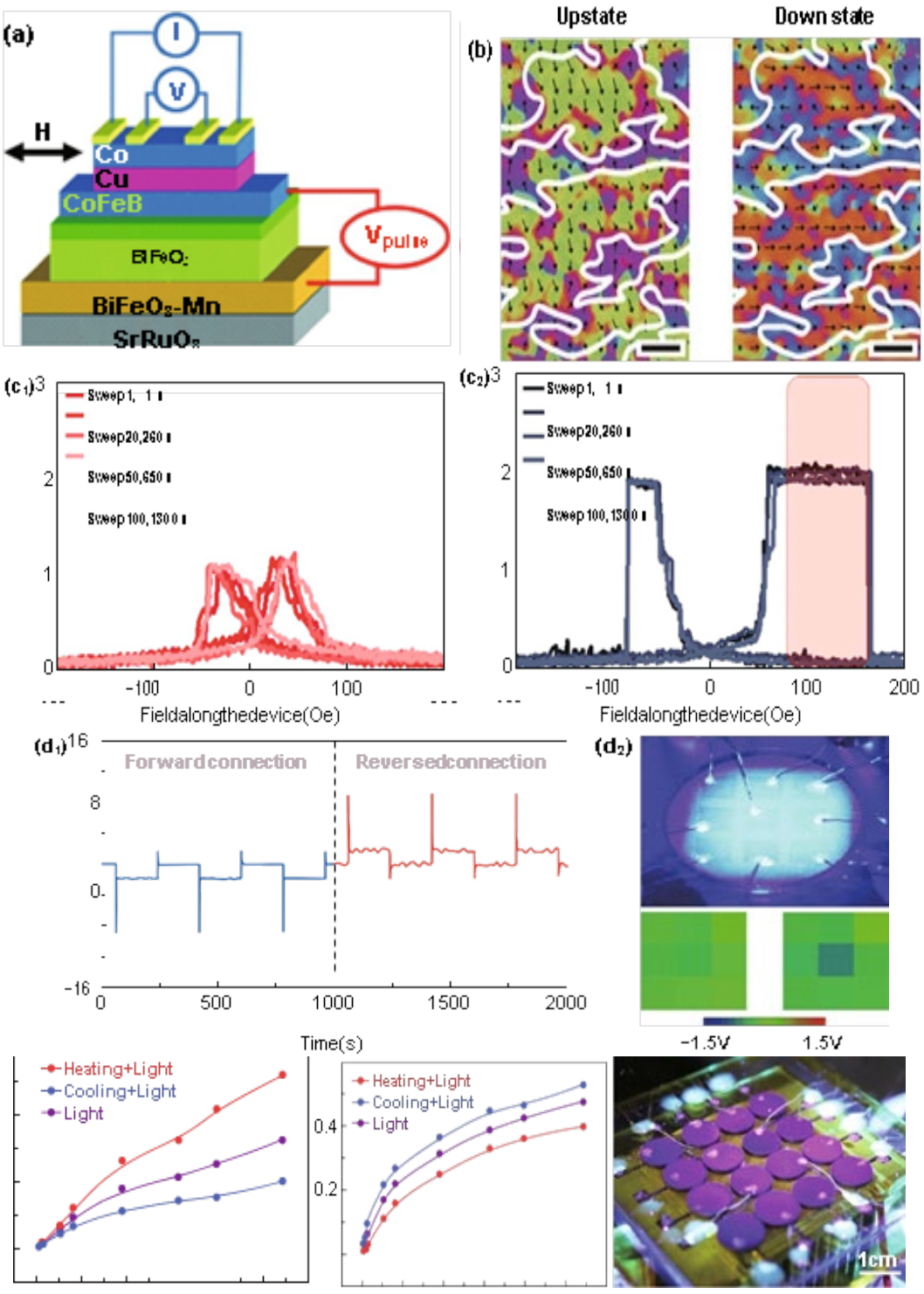

Fig. 11. Applications for spintronic and optic devices. Adapted by BFO

5. Conclusions

Recent advancements in nanomaterials have highlighted the exceptional properties of BFO, a multiferroic material known for its impressive characteristics such as high remnant polarization, magnetoelectric coupling at room temperature, and a relatively low bandgap.

In this study, Mn-Co modified BFO thin films were synthesized using a straightforward sol-gel technique. Comprehensive analyses were performed on the magnetic attributes, surface morphologies, and structural connections of the materials, revealing that all samples possess a rhombohedral polycrystalline structure. XRD and Raman spectroscopy confirmed the optimal incorporation of Co3+ and Mn3+ ions into the BFO lattice, while SEM imaging demonstrated that Mn-Co doping facilitates uniform particle growth and reduces grain size. Recent studies have shown that Co substitution in thin films can significantly enhance magnetic properties through noticeable agglomerations with smaller grain sizes. Vibrating Sample Magnetometer (VSM) evaluations reveal that these magnetic attributes are greatly improved, with the thin films of BF/Mn-C0.08O and BF/Mn-C0.10O achieving impressive Mr and Ms values of 3.68 and 47.84 emu/cm^3, respectively.

This enhancement is attributed to factors such as reduced oxygen defects, denser accumulations, improved super exchange interactions, and the structure breakdown of spiral-spin systems. However, challenges remain in developing new devices as ferroelectric and magnetoelectric performances still require further optimization, despite the high polarizations observed in BF/Mn-CO.

References

[1] R. Guo, L. You, Y. Zhou, Z.S. Lim, X. Zou, L. Chen, R. Ramesh, J.L. Wang, Nat. Commun. 4, 1990 (2013); https://doi.org/10.1038/ncomms2990

[2] J. Qi, N. Ma, Y. Yang, Adv. Mater. Interfaces 5, 1701189 (2018); https://doi.org/10.1002/admi.201701189

[3] J. Qi, N. Ma, X.C. Ma, R. Adelung, Y. Yang, ACS Appl. Mater. Interfaces 10, 13712- 13719 (2018); https://doi.org/10.1021/acsami.8b02543

[4] J. Ma, J. Ma, Q. Zhang, R. Peng, J. Wang et al., Nat. Nanotechnol. 13, 947-952 (2018); https://doi.org/10.1038/s41565-018-0204-1

[5] F. Mushtaq, X. Chen, M. Hoop, H. Torlakcik, E. Pellicer et al., iScience 4, 236-246 (2018); https://doi.org/10.1016/j.isci.2018.06.003

[6] H. Singh, K.L. Yadav, Ceram. Int. 41, 9285-9295 (2015); https://doi.org/10.1016/j.ceramint.2015.03.212

[7] C.R. Foschini, M.A. Ramirez, S.R. Simoes, J.A. Varela, E. Longo, A.Z. Simoes, Ceram. Int. 39, 2185-2195 (2013); https://doi.org/10.1016/j.ceramint.2012.08.083

[8] Dong, W.; Guo, Y.; Guo, B.; Liu, H.; Li, H.; Liu, H., Mater. Lett. 2012, 88, 140-142; https://doi.org/10.1016/j.matlet.2012.08.006

[9] Peng, Z.; Liu, B., Phys. Status Solidi A 2014, 2, 1-4; https://doi.org/10.1002/pssa.201431512

[10] Katiyar, R.K.; Sharma, Y.; Misra, P.; Puli, V.S.; Sahoo, S.; Kumar, A.; Scott, J.F.; Morell, G.; Weiner, B.R.; Katiyar, R.S., Appl. Phys. Lett. 2014, 105, 172904; https://doi.org/10.1063/1.4900755

[11] Wang, Z.; Cao, D.; Wen, L.; Xu, R.; Obergfell, M.; Mi, Y.; Zhan, Z.; Nasori, N.; Demsar, J.; Lei, Y., Nat. Commun. 2016, 7, 10348; https://doi.org/10.1038/ncomms10348

[12] Wu, J.; Fan, Z.; Xiao, D.; Zhu, J.; Wang, J., Prog. Mater. Sci. 2016, 84, 335-402; https://doi.org/10.1016/j.pmatsci.2016.09.001

[13] Khomchenko, V.A.; Karpinsky, D.V.; Paixão, J.A., J. Mater. Chem. C 2017, 5, 3623-3629; https://doi.org/10.1039/C7TC00833C

[14] Mao, W.; Wang, X.; Chu, L.; Zhu, Y.; Wang, Q.; Zhang, J.; Yang, J.; Li, X.; Wei, H. Phys.

Chem. Chem. Phys. 2016, 18, 6399-6405; https://doi.org/10.1039/C5CP07327H

[15] Dutta, D.P.; Tyagi, A., Appl. Surf. Sci. 2018, 450, 429-440; https://doi.org/10.1016/j.apsusc.2018.04.202

[16] Qiu, H.; Chen, G.; Fan, R.; Cheng, C.; Hao, S.; Chen, D.; Yang, C., Chem. Commun. 2011, 47, 9648; https://doi.org/10.1039/c1cc13707g

[17] Rong, Q.-Y.; Wang, L.-L.; Xiao, W.-Z.; Xu, L., Phys. B Condens. Matter 2015, 457, 1-4; https://doi.org/10.1016/j.physb.2014.08.028

[18] Marzouki, A.; Harzali, H.; Loyau, V.; Gemeiner, P.; Zehani, K.; Dkhil, B.; Bessais, L.; Megriche, A., Mater. 2018, 145, 316-321; https://doi.org/10.1016/j.actamat.2017.11.055

[19] Liu, Y.; Qi, J.; Zhang, Y.; Wang, Y.; Feng, M.; Zhang, J.; Wei, M.; Yang, J., Appl. Surf. Sci. 2018, 427, 745-752; https://doi.org/10.1016/j.apsusc.2017.08.083

[20] Sahni, M.; Mukaherjee, S.; Hamid, A.; Kumar, D.; Chauhan, S.; Kumar, N. J. Mater. Sci. Mater. Electron. 2020, 31, 7798-7810; https://doi.org/10.1007/s10854-020-03318-6

[21] Li, L.; Salvador, P.A.; Rohrer, G.S., Nanoscale 2014, 6, 24-42; https://doi.org/10.1039/C3NR03998F